

# UC Office of the President

## Recent Work

### Title

Neutrino capture and [Formula Presented]-process nucleosynthesis

### Permalink

<https://escholarship.org/uc/item/5rb3z9x5>

### Journal

Physical Review C - Nuclear Physics, 58(6)

### ISSN

0556-2813

### Authors

Meyer, BS  
McLaughlin, GC  
Fuller, GM

### Publication Date

1998

### DOI

10.1103/PhysRevC.58.3696

Peer reviewed

## Neutrino capture and $r$ -process nucleosynthesis

Bradley S. Meyer

*Department of Physics and Astronomy, Clemson University, Clemson, South Carolina 29634-1911*

Gail C. McLaughlin

*University of Washington, Institute for Nuclear Theory, Box 351550, Seattle, Washington 98195-1550*

George M. Fuller

*Department of Physics, University of California, San Diego, La Jolla, California 92093-0319*

(Received 28 April 1998)

We explore neutrino capture during  $r$ -process nucleosynthesis in neutrino-driven ejecta from nascent neutron stars. We focus on the interplay between charged-current weak interactions and element synthesis, and we delineate the important role of equilibrium nuclear dynamics. During the period of coexistence of free nucleons and light and/or heavy nuclei, electron neutrino capture inhibits the  $r$ -process. At all stages, capture on free neutrons has a larger impact than capture on nuclei. However, neutrino capture on heavy nuclei by itself, if it is very strong, is also detrimental to the  $r$ -process until large nuclear equilibrium clusters break down and the classical neutron-capture phase of the  $r$ -process begins. The sensitivity of the  $r$ -process to neutrino irradiation means that neutrino-capture effects can strongly constrain the  $r$ -process site, neutrino physics, or both. These results apply also to  $r$ -process scenarios other than the neutrino-heated winds. [S0556-2813(98)05012-2]

PACS number(s): 26.30.+k, 26.45.+h, 13.15.+g, 14.60.Lm

### I. INTRODUCTION

It has long been known that the  $r$ -process of nucleosynthesis is responsible for roughly half the solar system's supply of heavy nuclei [1,2]. Nevertheless, the astrophysical site or sites of the  $r$ -process remain a great mystery. The high neutron densities and rapid time scales associated with the  $r$ -process suggest core-collapse (type II or type Ib) supernovae as the most likely setting, but the exact environment within supernovae is unclear. The most plausible environment yet proposed is the neutrino-heated ejecta from the nascent neutron star [3–7]. Neutrinos from the Kelvin-Helmholtz-cooling neutron star heat matter strongly. Given sufficient heating, this material can escape the deep gravitational well and travel into interstellar space along with the rest of the stellar ejecta. Necessarily, this neutrino heating drives the entropy per nucleon to a large value ( $\sim 100k$ , where  $k$  is Boltzmann's constant). Crucially for the  $r$ -process, the emerging electron antineutrinos come from deeper in the neutron star than the electron neutrinos. This results from the larger opacity of the latter in the interior of the neutron star. As the neutrinos and antineutrinos capture on free neutrons and protons in the heated ejecta, the hotter antineutrinos drive the matter neutron rich [8]. The high entropies, fast expansion, and neutron richness of the ejecta may provide the right conditions for making  $r$ -process nuclei. However, present supernova models with standard neutrino physics do not attain the extreme conditions needed to make the heaviest  $r$ -process isotopes. The necessary conditions conceivably could be realized by invoking general relativistic effects, though these models are finely tuned at best [9,10]. As we will argue, however, even if these necessary conditions could be attained, they are not *sufficient* to guarantee a viable  $r$ -process.

While neutrino interactions with nuclei are generally not

an important effect in stellar nucleosynthesis (apart from normal beta decay and electron capture), neutrinos so completely dominate the environment just outside a newly born neutron star that their effects must be included in nucleosynthesis calculations done in the context of neutrino-driven ejecta. Initially, the electron fraction above the surface of the neutron star is set primarily by electron neutrino and electron antineutrino capture on free nucleons. Other neutrino capture effects occur, however, and have been studied. Meyer *et al.* [4] included neutral-current spallation of neutrons from nuclei in one of their models. They found some smoothing of the resulting  $r$ -process distribution, but the overall effect on the  $r$ -process yields was small. This was also studied by Qian *et al.* [11]. Meyer [12] then showed that spallation of abundant  ${}^4\text{He}$  in wind trajectories studied by Woosley *et al.* [7] had a large, detrimental effect on the  $r$ -process. Fuller and Meyer [13] and McLaughlin, Fuller, and Wilson [14] studied charge-current interactions on free nucleons and nuclei during expansions of neutrino-heated ejecta. The key finding in those works was the strong “alpha effect” in which the electron fraction grows rapidly as  ${}^4\text{He}$  nuclei assemble in the presence of a large neutrino flux. We verify this effect in Sec. V, and show that of all neutrino effects, it has the largest impact on the  $r$ -process yields.

Neutrino capture on heavy nuclei in competition with nuclear beta decay provided limits on supernova dynamics from the  $r$ -process, although significant capture on the mass number  $A = 130$  peak was not necessarily excluded [13,15]. However, establishing steady weak flow (the analogue of steady beta flow) would require a long timescale ( $> 1$  s) and therefore many neutrino captures [15]. Following on these studies and work by Nadyozhin and Panov [16], Qian *et al.* [11] proposed that neutrino capture was needed to accelerate the  $r$ -process. The basic idea is that neutrino capture acts like beta decay in moving nuclei to higher charge. Faster move-

ment upward in charge is a faster  $r$ -process. This scenario would also require many neutrino captures.

We show in this paper that if neutrino capture on nuclei is significant compared to nuclear beta decay, then other effects will destroy the possibility of any  $r$ -processing at all. The basic reason for this is simple: neutrino capture on a free neutron is much faster than on a neutron bound inside a nucleus because the former has many more final states available. For example, the neutrino capture cross section of black body neutrinos with temperature  $T_{\nu_e} = 3.5$  MeV on a free neutron is about  $1.6 \times 10^{-41}$  cm<sup>2</sup>. The cross section for the same neutrinos on a neutron bound inside <sup>130</sup>Cd, a typical  $r$ -process nuclide, is about  $8.6 \times 10^{-43}$  cm<sup>2</sup>. During the  $r$ -process, the abundance of neutrons inside and outside nuclei are comparable; thus, capture of a neutrino by a heavy nucleus will be accompanied by ( $\sim 5-10$ ) captures on free neutrons. This strongly depletes the supply of free neutrons and limits the  $r$ -process. This process is similar to the alpha effect and is examined in Sec. V. Furthermore, as we show in Sec. VI, each neutrino capture on a free neutron leads to assembly of new heavy nuclei, further depleting the supply of free neutrons per seed nucleus.

In addition to these considerations, we show in Sec. VII that neutrino capture on heavy nuclei *alone*, if it is very strong, does not accelerate the  $r$ -process but rather strongly limits it. This surprising result comes about because of the quasiequilibrium nuclear dynamics in the early part of the matter expansion. We describe these nuclear dynamics in Sec. IV. A proper understanding of these effects is important for any who seek to use the  $r$ -process to constrain supernova neutrinos.

The strong sensitivity of the  $r$ -process to neutrino irradiation presents a great challenge. In particular, the effects we explore here constrain either the  $r$ -process site or neutrino physics. We present some remarks on the implications of our work in Sec. VIII. Preliminary results were presented in [17].

## II. NEUTRINO-CAPTURE CROSS SECTIONS

Electron neutrino and antineutrino capture on free neutrons ( $n$ ) and protons ( $p$ ),

$$\nu_e + n \rightarrow p + e^-; \quad (1)$$

$$\bar{\nu}_e + p \rightarrow n + e^+ \quad (2)$$

play an important role in an  $r$ -process environment with a large neutrino flux. In a supernova, antineutrinos have a higher average energy and a higher luminosity than neutrinos, causing the material in the neutrino-driven wind to be neutron rich. In the following sections we discuss additional effects which arise from the process in Eq. (1). We also consider effects stemming from electron neutrino and antineutrino capture on heavy nuclei,

$$\nu_e + (Z, A) \rightarrow (Z+1, A) + e^-; \quad (3)$$

$$\bar{\nu}_e + (Z, A) \rightarrow (Z-1, A) + e^+, \quad (4)$$

where  $Z$  is the nuclear charge and  $A$  the nuclear mass of species  $(Z, A)$ . Since the material undergoing synthesis is neutron rich, in general Eq. (3) has a larger impact than Eq.

(4). In this section we describe our calculations of the cross sections for these neutrino processes. We also discuss our estimates of neutrino-induced neutron emission processes, which have been included in the network calculations. In calculating all capture rates, we assume that the distribution of neutrinos coming from the proto-neutron star is Fermi-Dirac with zero chemical potential. Though the actual neutrino and antineutrino distribution functions will deviate somewhat from our assumed spectral form, this will not change our qualitative conclusions.

For typical neutrino energies in the supernova, the nuclear channels most important for electron neutrino and antineutrino capture are the allowed Fermi and Gamow-Teller transitions. The corresponding operators are

$$|M_F|^2 = \left| \langle \psi_f | C_V \sum_{i=1}^A \tau(i) | \psi_i \rangle \right|^2, \quad (5)$$

$$|M_{GT}|^2 = \left| \langle \psi_f | C_A \sum_{i=1}^A \sigma(i) \tau(i) | \psi_i \rangle \right|^2, \quad (6)$$

where the sums run over each of the  $A$  nucleons in the nucleus. The Gamow-Teller strength obeys the Ikeda sum rule,  $S_{\beta^-} - S_{\beta^+} = 3|N - Z|$ . For neutron-rich nuclei,  $S_{\beta^-}$  is the Gamow-Teller strength in the neutrino-capture direction, while  $S_{\beta^+}$  corresponds to the antineutrino capture direction. For very neutron-rich nuclei, the antineutrino capture direction is Pauli blocked,  $S_{\beta^+} = 0$ , so the corresponding transition rate is zero. In these cases, the rate of antineutrino capture is negligible in comparison with neutrino capture since there is no Fermi resonance in the  $\beta^+$  direction.

In order to fully determine the effect of neutrino interactions during the  $r$ -process we need rates, cross sections and particle emission probabilities for a wide range of nuclei. Although it would be desirable to use shell model and continuum random phase approximation (CRPA) calculations for each nucleus, this is clearly impossible at present. Therefore, we adopt a simpler, more feasible approach using the single particle shell model. Where possible, we have verified that our results agree within reasonable errors with more detailed calculations.

The matrix elements and capture rates are calculated as described in [13,18], with some improvements. Most of the Fermi strength and Gamow-Teller strength is often collected in resonances. The Fermi resonance is narrowly collected in a single state, while the Gamow-Teller resonance has a wider distribution. We have modified our calculation to account for this width. This alteration has a relatively small impact on the overall transition rates (see [18]), but can have a slightly larger impact on particle spallation, which is described below. Another modification is the inclusion of a full integration of the Coulomb wave correction factor in the phase space integral. Our network has also been extended to include proton-rich nuclei, although in a robust  $r$ -process, relatively few of these appear. In a few cases where comparison is possible, our results are in reasonable agreement with calculations done using CRPA [11].

In addition we have included neutrino-induced neutron emission processes. For the very neutron rich nuclei typical of the  $r$ -process, several neutrons will be emitted after

neutrino-induced excitations to the Gamow-Teller and Fermi resonances. We calculate the number of neutrons emitted by comparing the neutron separation energy plus kinetic energy of each emitted neutron to the excitation energy of the nucleus. An estimate of the kinetic energy of an emitted neutron is

$$\langle E \rangle \approx \frac{\int_0^{E^* - S_n} e^2 \rho(E^* - S_n - e) de}{\int_0^{E^* - S_n} e \rho(E^* - S_n - e) de}, \quad (7)$$

where the level density is  $\rho(e) \propto \exp[2(ae)^{1/2}]$  in the Fermi gas model. Here,  $E^*$  is the excitation energy of the nucleus,  $S_n$  is the neutron separation energy, and  $a$  is the Fermi gas constant. For multiple neutron emission, we examine the excited state and neutron separation energy of each successive daughter nucleus when calculating the average kinetic energy carried away by the neutrons. We adopt this approach over a wide range of nuclei. We have compared our results to the neutrino-induced neutron emission probabilities calculated with the statistical model [11] and found them to be in reasonable agreement.

### III. DETAILS OF THE FLUID DYNAMICS AND NETWORK CALCULATIONS

Our primary interest is to study the neutrino-capture effects in neutrino-heated ejecta from nascent neutron stars. The relevant fluid trajectories are then neutrino-driven winds. Such winds have been studied in several papers (e.g., [6,7,10,19]). A simple estimate of the wind parameters can be obtained by assuming a constant entropy and radiation-dominated outflow where the enthalpy per baryon is equated to the gravitational potential per baryon. With these assumptions and the additional assumption that the mass outflow rate ( $\dot{M} = 4\pi r^2 \rho v$ ) is constant with time, then it can be shown that the ejected matter expands homologously such that the radial outward velocity  $v$  is

$$v \propto r, \quad (8)$$

where  $r$  is the radial coordinate. Solution of Eq. (8) yields

$$r = r_0 \exp(t/\tau), \quad (9)$$

where  $r_0$  is the initial radius and  $\tau$  is the constant expansion time scale

$$\tau = r/v. \quad (10)$$

With the above assumption of constant entropy and an assumed  $\propto 1/r$  scaling for the enthalpy per baryon, the density  $\rho$  scales as

$$\rho \propto r^{-3}. \quad (11)$$

This follows because an equation of state completely dominated by relativistic particles has an entropy per baryon,

$$S \approx \frac{2\pi^2}{45} \frac{1}{N_A} g_s \frac{T^3}{\rho}, \quad (12)$$

where  $g_s$  is the effective relativistic particle statistical weight. In our numerical calculations, we include not only the relativistic photons in our equation of state but also the partially (in general) relativistic  $e^+ - e^-$  pairs and the non-relativistic nuclear species where appropriate. Including non-relativistic degrees of freedom in a reckoning of the entropy results in a somewhat different behavior for  $T$  than that given in Eq. (12) (see below).

We performed our calculations with the Clemson nucleosynthesis code [12,20,21]. This is a fully implicit, single-network code that includes over 3000 nuclear species ranging from neutrons and protons to actinide nuclei. The reaction network used for the present calculation included isotopes for each element from the proton-drip to the neutron-drip lines. We used neutrino-capture rates computed as in Sec. II. The neutrinos were taken to have Fermi-Dirac energy spectra with zero chemical potential and with temperatures  $kT_{\nu_e} = 3.5$  MeV and  $kT_{\bar{\nu}_e} = 4.0$  MeV. Because we are not studying neutral-current effects in this paper, we ignored the  $\mu$  and  $\tau$  neutrinos. The luminosity in electron neutrinos was taken to be  $10^{51}$  ergs/s while that of the electron antineutrinos was taken to be  $4 \times 10^{51}$  ergs/s. The large discrepancy in the electron neutrino and anti-neutrino luminosities was necessary to provide ejecta that were neutron rich enough to guarantee the *necessary* conditions for  $r$ -process nucleosynthesis to occur.

All of our calculations were performed at constant entropy. In the true expansion out-of-equilibrium nuclear reactions during the expansion generate entropy. Nevertheless, for sufficiently high entropy (greater than  $\sim 50k$  per nucleon) the generated entropy has little effect on the nuclear abundances [22]. Our technique was the following. We began with  $r_0 = 5.6$  km, an entropy of  $110k$  per nucleon, a density of  $2 \times 10^8$  g/cm<sup>3</sup>, and an expansion timescale  $\tau = 0.3$  s. This corresponded to an initial temperature of  $T_9 = T/10^9 \text{ K} \approx 40$ . The temperature and density track at this early stage has little effect on the resulting nucleosynthesis. We only extend the beginning of the calculation to such high temperatures to ensure that at  $T_9 = 10$  our nuclear reaction calculations begin with an electron fraction that accurately represents a steady state between neutrino and antineutrino capture rates, with a small contribution from electron and positron capture. At each time step  $t + \Delta t$ , we updated the radius  $r(t + \Delta t)$  [Eq. (9)] and density  $\rho(t + \Delta t)$  [Eq. (11)]. We then estimated the new temperature  $T(t + \Delta t)$  and updated the abundances  $Y(t + \Delta t)$  with the nuclear network. We next computed the entropy by inverting the relevant integral equations for the electron fraction and the entropy [22] and compared the new entropy at  $t + \Delta t$  with the old entropy at  $t$ . If the entropies at  $t$  and  $t + \Delta t$  did not agree, we tried a new temperature and repeated the procedure. Once we found  $T(t + \Delta t)$  such that the entropies agreed, we moved on to the next time step.

Figure 1 shows the trajectory for our reference calculation in which neutrinos were ‘‘turned off’’ after the matter had cooled below  $T_9 = 10$ . The solid line gives the actual temperature-time or temperature-radius relation while the dashed line gives the result for a purely  $\rho \propto T^3$  case. The actual network calculation does not follow the simple  $T \propto 1/r$  expected if  $\rho \propto T^3$ . Rather, there is heating of the matter due to  $e^+ - e^-$  annihilations from  $T_9 \approx 8 - 0.8$ , that is, from

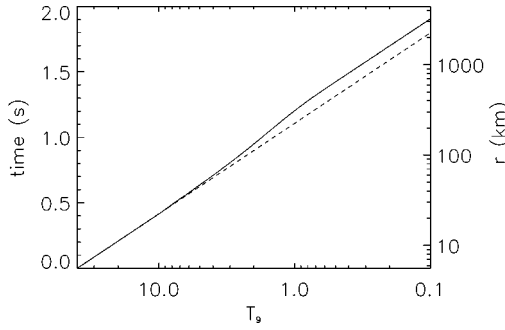


FIG. 1. The temperature-time or temperature-radius trajectory for the reference expansion (model 0), shown as the solid line. The dashed curve gives the trajectory for matter completely dominated by relativistic particles, for which  $\rho \propto T^3$  and  $T \propto 1/r$ . The reheating in the reference expansion results from the annihilation of electron-positron pairs, just as in the early universe.

about 0.5–1.2 seconds in the expansion. This is precisely analogous to the electron-positron annihilation that occurred in the early universe. This is also evident in Fig. 2, which shows the entropies in the leptons, photons, and nuclear species during the expansion. The leptons transfer their entropy into the photons rather dramatically, especially around  $T_9 = 3-2$ , as the pairs annihilate. The decline in entropy in nucleons results from nuclear reactions that lock free nucleons into nuclei, thereby reducing the number of degrees of freedom per nucleon. The gradual drop in the entropy in nuclear species from  $T_9 = 2$  down to  $T_9 < 0.2$  signals the classical  $r$ -process phase in which free neutrons are being incorporated into heavy nuclei. The calculation proceeded until the abundance  $Y_n$  of free neutrons per baryon dropped to below  $10^{-20}$ .

With our chosen conditions, final reaction freezeout occurred at  $T_9 \approx 0.5$ , a radius  $r \approx 1000$  km, and a density of about 35 g/cc. A faster expansion could lead to freezeout at an even greater radius and smaller density. A very fast expansion potentially poses problems for the  $r$ -process. As discussed above, wind matter may expand homologously such

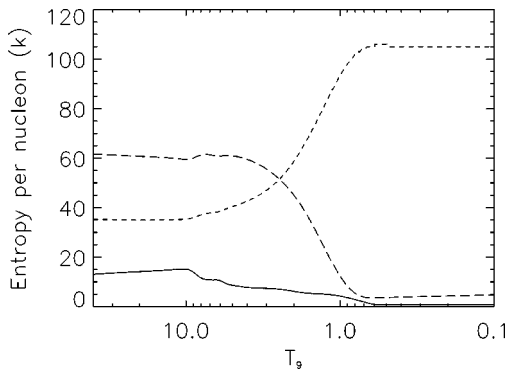


FIG. 2. The entropy per nucleon in units of Boltzmann’s constant  $k$  in nuclear species (solid curve), photons (short-dashed curve), and leptons (long-dashed curve) during the reference expansion. The entropy is a constant throughout the expansion, so the constituent entropies always sum to  $110k$  per nucleon. The pair annihilation between  $T_9 \approx 3$  and  $T_9 \approx 1$  shifts entropy from the leptons to the photons. The entropy in nuclear species declines as free nucleons lock up into heavier species. This decreases the number of degrees of freedom per nucleon.

that the outflow velocity is proportional to the radial distance from the neutron star. In such a case, the density of a wind element falls exponentially with the time. This means the density could be declining so rapidly that the  $r$ -process would freeze out before all the neutrons could be incorporated into nuclei. The perceived need to circumvent this freezeout problem by accelerating the  $r$ -process with neutrino capture motivated some of the previous studies of neutrino capture during the  $r$ -process.

The next sections will show that rapid neutrino capture certainly would solve this potential problem, but at the rather drastic cost of eliminating the possibility of the  $r$ -process in the first place. On the other hand, for the  $r$ -process to successfully occur in neutrino-heated ejecta, matter must travel out sufficiently rapidly to escape the harmful effects of the neutrinos. This would appear to call for a very rapid expansion with the attendant difficulty of freeze-out before successful incorporation of neutrons into nuclei. The solution to this dilemma is likely to be that neutrino-driven winds cannot continue to accelerate so rapidly that the nuclear reactions would freeze out before the  $r$ -process finished. Neutron capture can occur rapidly even in relatively cold matter down to densities of order 1–10 g/cc, and it is unlikely that neutron star matter would be able to expand homologously from neutron star densities down to this low value. At some distance the acceleration provided by the neutrinos declines and the matter from then on would travel out with a more or less constant velocity. In this case the density declines only as the inverse square of the time for constant mass loss. This is much slower and would allow the  $r$ -process to occur.

#### IV. THE $r$ -PROCESS

Before presenting the details of the nucleosynthesis calculations, it is useful to review the basics of the  $r$ -process. A proper understanding helps clarify neutrino effects.

The nuclear dynamics of matter expanding from high density and temperature is probably best viewed as a descent of the hierarchy of statistical equilibria [21]. Each equilibrium is an entropy maximum subject to some number of constraints on the nuclear populations. The top of the hierarchy is the equilibrium with the fewest constraints. As the matter expands and cools, some nuclear reaction becomes too slow to maintain that equilibrium. This imposes a new constraint on the equilibrium. With further expansion, other reactions become too slow, and new constraints appear. Reaction freeze-out occurs when there are the maximum possible number of constraints on the nuclear populations. It is useful to note that the greater the number of constraints, the greater the order. Order emerges in such systems as the number of states available to the system increasingly falls short of the maximum possible.

In the  $r$ -process, matter can begin at sufficiently high temperature and density that the nuclei are in weak statistical equilibrium (WSE). Here all strong, electromagnetic, and weak interactions among nuclei proceed sufficiently rapidly that the only constraints on the equilibrium are that charge neutrality holds and that the baryon and lepton numbers are fixed, as is the energy if the matter comprises an isolated system. To find the particle abundances in this equilibrium, it is only necessary to specify the temperature  $T$  and density  $\rho$ .

An entropy maximization via Lagrange multipliers yields beta equilibrium

$$\mu_p + \mu_{e^-} = \mu_n + \mu_{\nu_e}, \quad (13)$$

where the different  $\mu$ 's are (total energy) chemical potentials for protons, electrons, neutrons, and electron-type neutrinos, respectively. This equation indicates equilibrium in the inter-conversion of neutrons and protons by the weak interactions induced by electrons and/or positrons and electron neutrinos and/or electron antineutrinos. Another result is

$$\mu_{e^+} = -\mu_{e^-}, \quad (14)$$

which indicates, for example, electromagnetic equilibrium between electrons and positrons. Finally, the chemical potential for nuclear species  $(Z,A)$  with charge number  $Z$  and mass number  $A$  satisfies

$$\mu(Z,A) = Z\mu_p + N\mu_n, \quad (15)$$

where  $N = A - Z$  is the neutron number for that species. The ideal Boltzmann gas expression for the chemical potential of the nuclear species is

$$\mu(Z,A) = m(Z,A)c^2 + kT \ln\left(\frac{Y(Z,A)}{Y_Q(Z,A)}\right), \quad (16)$$

where  $m(Z,A)$  is the mass of nuclear species  $(Z,A)$ ,  $k$  is Boltzmann's constant,  $T$  is the temperature,  $Y(Z,A)$  is the abundance per nucleon of  $(Z,A)$ , and  $Y_Q(Z,A)$  is the quantum abundance of nucleus  $(Z,A)$  per nucleon.  $Y_Q(Z,A)$  is given by

$$Y_Q(Z,A) = \left(\frac{m(Z,A)kT}{2\pi\hbar^2}\right)^{3/2} \frac{G(Z,A)}{\rho N_A}, \quad (17)$$

where  $G(Z,A)$  is the nuclear partition function of  $(Z,A)$  and  $N_A$  is Avogadro's number. It is useful to note that the quantum concentration  $n_Q(Z,A) = \rho N_A Y_Q(Z,A)$  is the number density associated with one nucleus  $(Z,A)$  in a cube of side roughly equal to the thermal average de Broglie wavelength of that nucleus. The resulting nuclear abundances per nucleon are then (see [1])

$$Y(Z,A) = Y_Q(Z,A) \left(\frac{Y_p}{Y_{Qp}}\right)^Z \left(\frac{Y_n}{Y_{Qn}}\right)^N \exp(B(Z,A)/kT), \quad (18)$$

where the nuclear binding energy  $B(Z,A)$  of species  $(Z,A)$  is

$$B(Z,A) = Zm_p c^2 + Nm_n c^2 - m(Z,A) c^2. \quad (19)$$

The first reactions to become too slow to maintain full equilibrium during the expansion are usually the weak interactions. First the electron and positron capture reactions drop out of equilibrium. Since the electron neutrino and antineutrino capture reactions drop out later, the electron fraction is essentially determined by the neutrino reactions. After the weak reactions become slow, the electron-to-nucleon fraction  $Y_e$  is not its WSE value and must now be specified.  $Y_e$  is given from charge neutrality by

$$Y_e = \sum_{Z,A} ZY(Z,A), \quad (20)$$

where the sum runs over all nuclear species including free nucleons. All other reactions proceed rapidly to maintain equilibrium. This new equilibrium, nuclear statistical equilibrium (NSE), is an entropy maximum just like WSE, but now has the extra constraint on  $Y_e$ . The NSE abundances are given by Eq. (18), but these must now satisfy Eq. (20) in place of Eq. (13). The extra constraint on NSE locates it lower in the hierarchy of statistical equilibria than WSE. It is important to understand that the constraint on  $Y_e$  does not mean it is fixed in time, rather that it changes more slowly than needed to maintain WSE. All other reactions are occurring rapidly.

The next reactions during the expansion to become too slow are usually the three-body reactions that assemble alpha particles into heavier nuclei. In the neutron-rich matter required for the  $r$ -process, these reactions are triple- $\alpha$  ( $\alpha + \alpha + \alpha \rightarrow {}^{12}\text{C}$ ) and the  ${}^9\text{Be}$  sequence [ $\alpha + \alpha + n \rightarrow {}^9\text{Be}$  followed by  ${}^9\text{Be}(\alpha, n){}^{12}\text{C}$ ]. Among strong and electromagnetic reactions, these can be the slowest because they require three instead of the usual two particles to collide. The slowness of these reactions keeps the system from maintaining  $Y_h$ , the abundance of heavy nuclei (i.e. those nuclei with  $A \geq 12$ ), at the full equilibrium value. The definition of  $Y_h$  is

$$Y_h = \sum_{Z,A \geq 12} Y(Z,A), \quad (21)$$

and the slowness of the three-body reactions now constrains  $Y_h$  to a specified value. Nevertheless, all other strong and electromagnetic reactions proceed rapidly. The resulting equilibrium is called quasiequilibrium (QSE) [23]. In it, heavy nuclei are all in equilibrium with each other under the exchange of light particles ( $n, p, \alpha$ ), although the number of heavy nuclei differs from that in NSE. The abundances in QSE are given by [21]

$$Y^{QSE}(Z,A) = e^{\mu_h/kT} R_p^Z R_n^N Y^{NSE}(Z,A), \quad (22)$$

where  $\mu_h$  is the chemical potential of heavy nuclei (the energy required to add a new heavy nucleus at constant entropy),  $R_p = Y_p/Y_p^{NSE}$  and  $R_n = Y_n/Y_n^{NSE}$  are the overabundances of neutrons and protons compared to NSE, and  $Y^{NSE}(Z,A)$  is the NSE abundance of  $(Z,A)$  at the same  $T$ ,  $\rho$ , and  $Y_e$  as the QSE. The QSE abundances must satisfy baryon number conservation and Eqs. (20) and (21), which give three equations to solve for the three unknowns  $\mu_h$ ,  $R_p$ , and  $R_n$ . It is possible to use Eq. (20) in solving for the QSE or NSE solutions at a given instant of time even though the (out-of-equilibrium)  $Y_e$  is changing, as long as it is changing on a timescale slow compared to that for the reactions in equilibrium. The same is true for Eq. (21) and a slowly changing  $Y_h$  in QSE.

A clear picture of the QSE aspect of the expansion of  $r$ -process matter is important for understanding the effects of neutrino capture. One might suppose that neutrino capture on neutron-rich nuclear species simply increases the average nuclear charge. In a QSE, however, the nuclei are all interlocked in a large competitive equilibrium, and the abun-

dances are set by a Darwinian struggle among the species. The “fittest” species tend to win (i.e. have large abundances), and these are nuclei with strong nuclear binding. Neutrino capture increases  $Y_e$ . An increase of  $Y_e$  leads to more proton-rich nuclei in QSE. Protons would be less bound in such nuclei, so it is possible that the QSE could adjust itself by disintegrating some protons from nuclei which would thereby lower the average nuclear charge. It is only after the QSE breaks down that neutrino capture would unambiguously increase the average nuclear charge. We illustrate these effects in Sec. VII.

The large QSE among all heavy nuclei breaks down when certain reactions among the heavy species become too slow to maintain the equilibrium. At this point the nuclear system breaks up into smaller QSE clusters. The nuclei within these clusters are in equilibrium under exchange of light particles, but the clusters are not in equilibrium with each other. Now the number of nuclei in each cluster is slowly changing and must be specified. The abundances of species in cluster  $j$  are then

$$Y^{(j)}(Z,A) = e^{\mu_h^{(j)}/kT} R_p^Z R_n^N Y^{\text{NSE}}(Z,A), \quad (23)$$

where  $\mu_h^{(j)}$  is the energy required to add a nucleus into cluster  $j$  at constant entropy.

As more of the nuclear reactions become slow due to the cooling, more QSE clusters appear. For neutron-rich matter, the QSE clusters tend to break up into isotopic chains of a given  $Z$ , that is, clusters of nuclei in equilibrium under the exchange of neutrons but not protons or alpha particles. This is the so-called  $(n, \gamma) - (\gamma, n)$  equilibrium of the classical  $r$ -process phase. Charged-particle strong and electromagnetic reactions have become too slow, so nuclei can only move from one  $Z$  to the next now by either nuclear beta decay or neutrino capture. The abundances in an  $(n, \gamma) - (\gamma, n)$  equilibrium isotopic chain are simply found from Eq. (23) since these nuclei all belong to the same QSE cluster:

$$\frac{Y(Z,A+1)}{Y(Z,A)} = \left( \frac{Y_n}{Y_{Qn}} \right) \left( \frac{m(Z,A+1)}{m(Z,A)} \right)^{3/2} \exp(S_n(Z,A+1)/kT), \quad (24)$$

where the neutron separation energy  $S_n(Z,A+1)$  is given by

$$S_n(Z,A+1) = m(Z,A)c^2 + m_n c^2 - m(Z,A+1)c^2. \quad (25)$$

Equation (24) is the classic equation relating the abundances of neighboring isotopes in  $(n, \gamma) - (\gamma, n)$  equilibrium [1].

The  $(n, \gamma) - (\gamma, n)$  equilibrium eventually breaks down as neutron-capture and disintegration rates become too slow. Even smaller QSE clusters appear (typically as adjacent pairs of even and odd  $N$  isotopes), but these equilibria quickly break and the  $r$ -process freezes out. The neutron-rich nuclei simply beta decay back to the stability line.

Figure 3 illustrates some of these ideas. Shown are the elemental abundances for several temperatures during the reference expansion. The solid curve gives the abundances from the actual network calculations. The dashed curve shows the NSE abundances at the same temperature, density, and  $Y_e$  as in the network calculation, while the dotted curve gives the QSE abundances at the same temperature, density,

$Y_e$ , and  $Y_h$  as in the network calculation. By  $T_9=6.03$ , the nuclear populations have already fallen out of NSE because of the slowness of the three-body reactions assembling heavy nuclei. The abundances are, however, very accurately in QSE. The QSE is maintained through  $T_9=4.93$ , although the QSE and NSE are strongly diverging. By  $T_9=4.64$ , an abundance peak at  $Z=50$  is building up, but the network abundances are not keeping pace because of the slowness of the nuclear reactions that carry nuclei to higher charge. The nuclei have fallen out of the large QSE cluster that contained all of the heavy nuclei. A larger number of more restricted QSE clusters is now present, so the system has dropped in the hierarchy of statistical equilibria. By  $T_9=4.02$ , the abundance distribution is very different from that of the single large QSE. Interestingly, the abundances are dominated by the single isotope  $^{94}\text{Kr}$  with nearly 19% of the mass (the remaining mass is in free neutrons and alpha particles). This isotope serves as the initial seed nucleus for neutron captures during the subsequent “classical”  $r$ -process phase of the expansion. By  $T_9=2.98$ , some beta decays have already shifted matter to higher charge, but the  $r$ -process has only just begun. An mpeg movie of Fig. 3 is available for viewing at the web site <http://photon.phys.clemson.edu/movies.html> Other movies at that site show the development of QSE clusters and the evolution of the abundances.

## V. NUCLEOSYNTHESIS RESULTS

We ran a total of eight models. These are summarized in Table I. In all cases the initial conditions were those of the reference calculation (model 0) as were the neutrino temperatures and luminosities. In all cases, at  $T_9=10$  the material begins in weak steady state, which is set primarily by the neutrino and antineutrino capture reactions. Below  $T_9=10$ , the neutrino effects varied with the model. For example, in model 1, neutrino capture on free nucleons and nuclei was disabled below  $T_9=10$ , but neutrino capture on heavy nuclei was turned back on for  $T_9 \leq 3$ . For model 2, neutrino capture on both free nucleons and heavy nuclei was disabled below  $T_9=10$ , but both were turned back on for  $T_9 \leq 3$ . For model 3, neutrino capture occurred on free nucleons and heavy nuclei throughout the expansion.

We investigated in detail models 0 through 3 to see the effects of neutrino capture during the  $r$ -process. Figure 4 shows the final abundances versus nuclear mass number for each of these models. There is only a slight difference between models 0 (no neutrino effects below  $T_9=10$ ) and 1 (neutrino capture on heavy nuclei below  $T_9=3$ ). The curves show strong  $A=130$  and  $A=195$  abundance peaks, with the latter larger in abundance. These models have experienced a robust  $r$ -process. By contrast, model 2 (neutrino capture on heavy nuclei and free nucleons below  $T_9=3$ ) shows an  $A=130$  abundance peak, but neutrino captures on free nucleons during the  $r$ -process phase has prevented the run up to  $A=195$ . Finally, model 3 (neutrino capture on heavy nuclei and free nucleons on throughout the expansion) shows no  $r$ -process. The mass is largely concentrated in three nuclear species  $^{88}\text{Sr}$ ,  $^{89}\text{Y}$ , and  $^{90}\text{Zr}$ . Neutrino capture has completely prevented the  $r$ -process in this case.

The “success” of an  $r$ -process expansion in making heavy species depends on  $R$ , the ratio of the abundance of

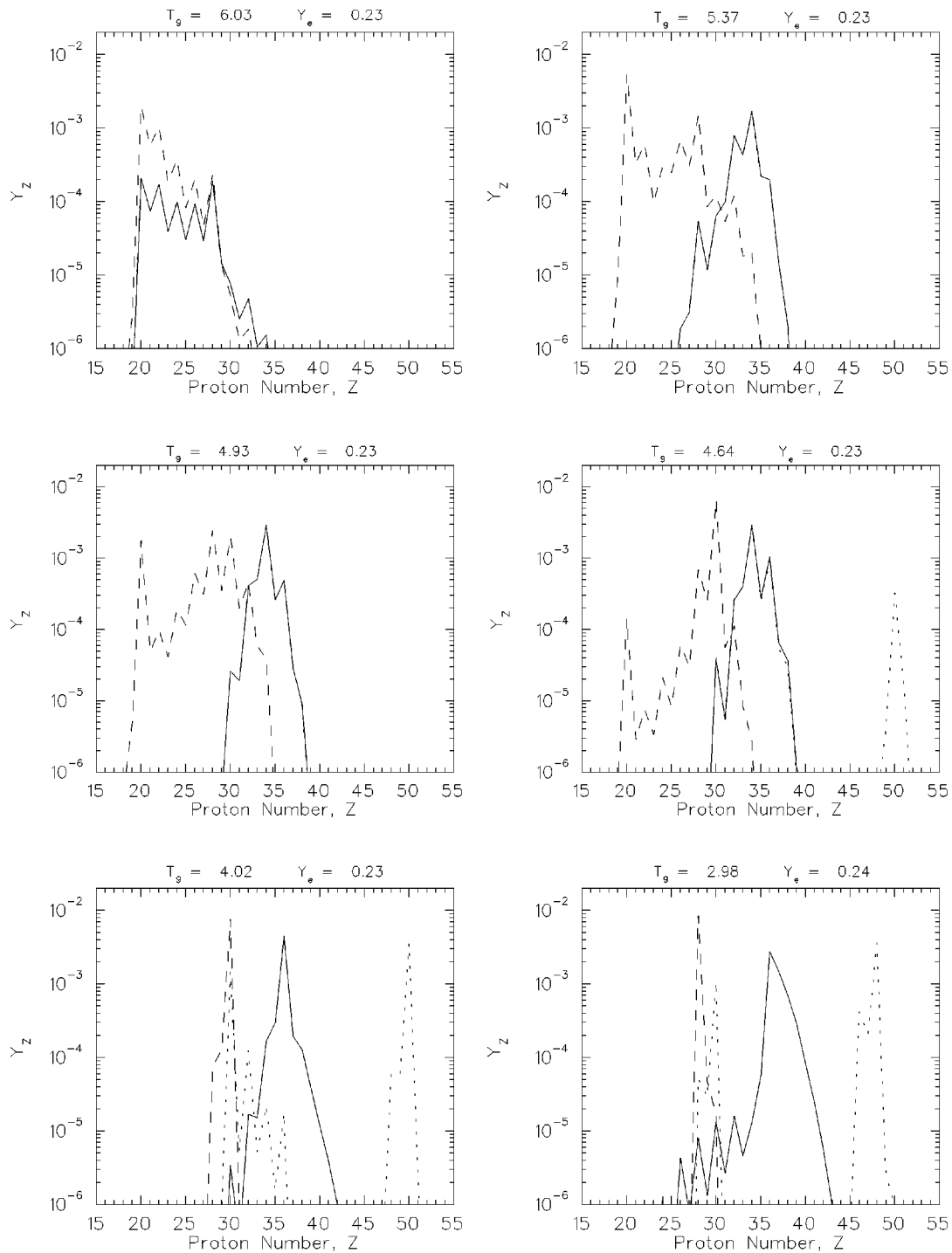


FIG. 3. The elemental abundances at six instants during the reference expansion. In each panel, the solid curve gives the abundances from integration of the nuclear reaction network. The dashed curve shows the NSE abundances for the same temperature, density, and  $Y_e$  as in the network calculation. The dotted curve shows the QSE abundances for the same temperature, density,  $Y_e$ , and  $Y_h$  as in the network calculation. By  $T_9=6.03$ , the abundances have already fallen out of NSE. However, they remain in QSE down below  $T_9=5$ . As the QSE distribution shifts to higher charge, the actual abundances cannot keep pace, and the system falls further in the hierarchy of statistical equilibria. More QSE clusters develop. The system eventually breaks down into  $(n, \gamma) - (\gamma, n)$  equilibrium in which nuclei are in equilibrium only under exchange of neutrons. This is the “classical”  $r$ -process phase of the expansion.

free neutrons to that of the heavy seed nuclei that capture those free neutrons during the  $r$ -process. The larger  $R$  is, the more neutrons each nucleus will capture on average, and, consequently, the heavier the final nuclei produced. Figure 5 shows  $R$  in models 0 through 3. In models 0, 1, and 2,  $R$  is about 70 at  $T_9=3$ , roughly the beginning of the  $r$ -process

phase of the expansion. Since the average heavy nucleus has mass number  $\sim 100$  at this point, the final average heavy nucleus has a mass number  $\sim 170$ . In the reference calculation (model 0),  $R$  declines gradually as the temperature falls. This is due to the capture of neutrons by nuclei during the  $r$ -process. Model 1 follows suit, although the neutrino cap-



TABLE I. Parameters for our eight model calculations. For all calculations, the entropy was a constant  $110k$  per nucleon and  $T_{\nu_e} = 3.5$  MeV and  $T_{\bar{\nu}_e} = 4.0$  MeV.

Model	$L_{\nu_e}$ (ergs/s)	$L_{\bar{\nu}_e}$ (ergs/s)	$\nu_e, \bar{\nu}_e$ -capture on free nucleons	$\nu_e, \bar{\nu}_e$ -capture on nuclei	Other comments
0	$10^{51}$	$4 \times 10^{51}$	for $T_9 \geq 10$	No	Reference calculation
1	$10^{51}$	$4 \times 10^{51}$	for $T_9 \geq 10$	for $T_9 \geq 10$ and $T_9 \leq 3$	—
2	$10^{51}$	$4 \times 10^{51}$	for $T_9 \geq 10$ and $T_9 \leq 3$	for $T_9 \geq 10$ and $T_9 \leq 3$	—
3	$10^{51}$	$4 \times 10^{51}$	On throughout	On throughout	Most realistic
4	$10^{51}$	$4 \times 10^{51}$	for $T_9 \geq 10$ and $T_9 \leq 3$	for $T_9 \geq 10$ and $T_9 \leq 3$	No ${}^3\text{H}(\alpha, \gamma){}^7\text{Li}$
5	$10^{52}$	$4 \times 10^{52}$	for $T_9 \geq 10$	for $T_9 \geq 10$ and $T_9 \leq 7$	—
6	$10^{52}$	$4 \times 10^{52}$	for $T_9 \geq 10$	for $T_9 \geq 10$ and $T_9 \leq 5$	—
7	$10^{52}$	$4 \times 10^{52}$	for $T_9 \geq 10$	for $T_9 \geq 10$ and $T_9 \leq 3$	—

ture by heavy nuclei for  $T_9=3$  slightly enhances the rate of increase of nuclear charge and thereby lowers  $R$  a little for each temperature. In model 2, however,  $R$  plummets drastically once the neutrino captures are enabled below  $T_9=3$ . The only difference between models 1 and 2 is that model 2 includes neutrino capture on free nucleons which must therefore be the cause of the large drop in  $R$ . Finally, in model 3,  $R$  drops to zero before the  $r$ -process can even begin.

The effects of neutrino capture are also apparent in Fig. 6, which shows  $Y_e$  for models 0 through 3.  $Y_e$  is set early in the

expansion by the interactions of neutrinos and anti-neutrinos with free neutrons and protons. The antineutrinos, which capture on protons to make neutrons, have a higher temperature and luminosity than the neutrinos, which convert neutrons into protons. This gives rise to the low steady-state value of  $Y_e$ . For model 0,  $Y_e$  stays low until the  $r$ -process begins at about  $T_9=3$ , then  $Y_e$  rises due to the nuclear beta decays that increase the nuclear charge. Model 1 shows similar behavior, although  $Y_e$  increases slightly faster due to the added effect of neutrino capture on heavy nuclei. By con-

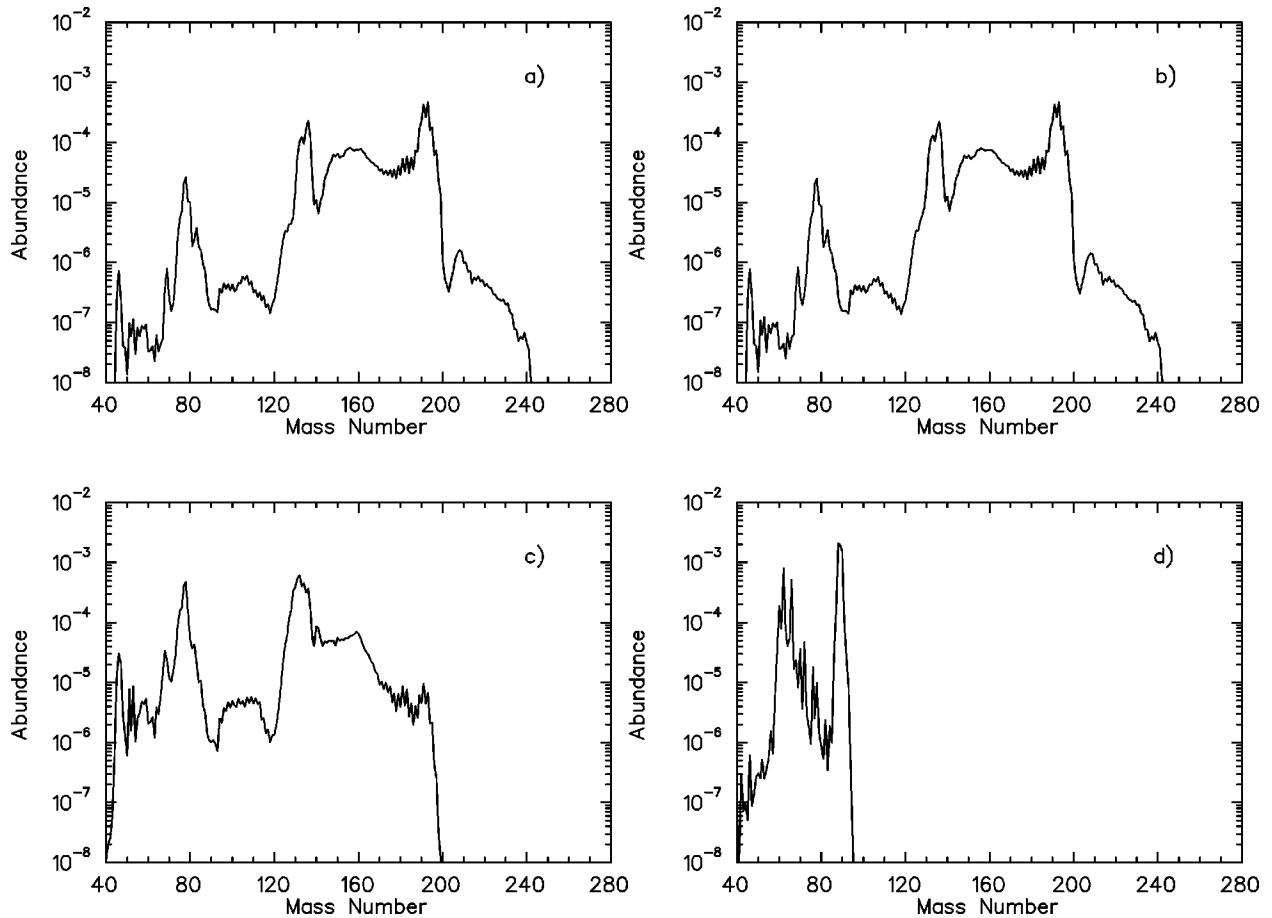


FIG. 4. Final mass fractions as a function of nuclear mass number for (a) model 0 (the reference calculation), (b) model 1 (neutrino and anti-neutrino capture only on heavy nuclei for  $T_9 \leq 3$ ), (c) model 2 (neutrino and antineutrino capture on free nucleons and heavy nuclei for  $T_9 \leq 3$ ), and (d) model 3 (neutrino and antineutrino capture on free nucleons and nuclei throughout the expansion). A robust  $r$ -process has occurred for models 0 and 1 allowing production of the  $A=195$  peak nuclei. In model 2, the resulting  $r$ -process is less robust—the  $A=195$  peak is not present. In model 3 there is no production of heavy  $r$ -process nuclei.

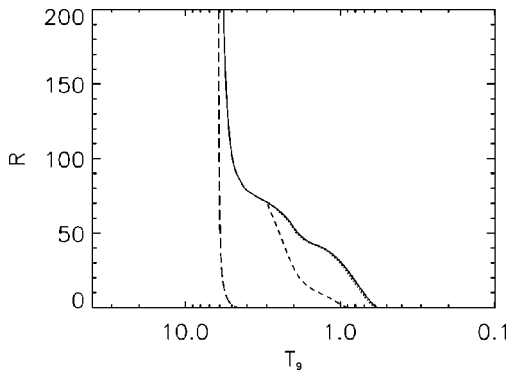


FIG. 5. The neutron-to-seed ratio  $R$  in models 0 (solid curve), 1 (dotted curve), 2 (short-dashed curve), and 3 (long-dashed curve). Neutrino capture on free nucleons strongly reduces  $R$  during the expansion and thereby hampers the  $r$ -process.

trast, model 2 shows a much more rapid rise in  $Y_e$  below  $T_9=3$ . Again, this is due to neutrino capture on free neutrons. We note that the number of free neutrons per nucleon at  $T_9=3$  is 0.38 while the number of neutrons locked up into heavy nuclei is 0.34. A neutrino capture by either a bound or free neutron increases  $Y_e$  by the same amount, and the number of bound and free neutrons is about the same. The rather strong difference between models 1 and 2 is due to the much larger cross section for neutrino capture on free neutrons than on bound neutrons due to the larger number of final states available to the former. Neutrino capture on a free neutron decreases the number of neutrons available for incorporation into nuclei. For these simple reasons, neutrino capture during the  $r$ -process on balance must hinder the production of high-mass nuclei. Model 3 shows an even more dramatic rise in  $Y_e$ . For this model,  $Y_e$  quickly rises to about 0.45 and changes little for the rest of the expansion. This drastic behavior partly reflects the classic alpha effect identified in [13,14].

Neutrino capture on free neutrons does not simply hinder

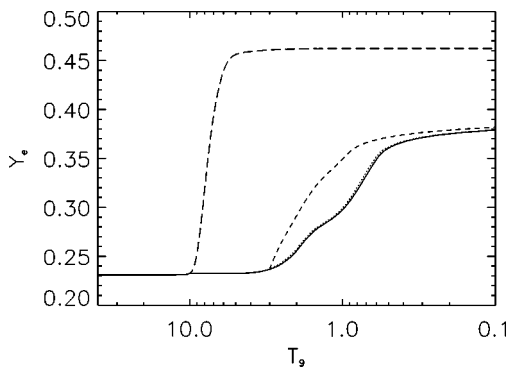


FIG. 6. The electron fraction  $Y_e$  for models 0 (solid curve), 1 (dotted curve), 2 (short-dashed curve), and 3 (long-dashed curve). In the reference expansion (model 0),  $Y_e$  starts to grow as the  $r$ -process phase of the nucleosynthesis begins for  $T_9 < 3$ . It rises due to nuclear beta decays. From model 1, it is apparent that neutrino captures on heavy nuclei slightly enhance  $Y_e$  during the expansion. Model 2, however, shows that neutrino capture on free neutrons (for  $T_9 < 3$ ) has a much larger effect on  $Y_e$  than capture on heavy nuclei. Model 3 shows that neutrino capture on free neutrons early has an even greater influence due to the “alpha effect.”

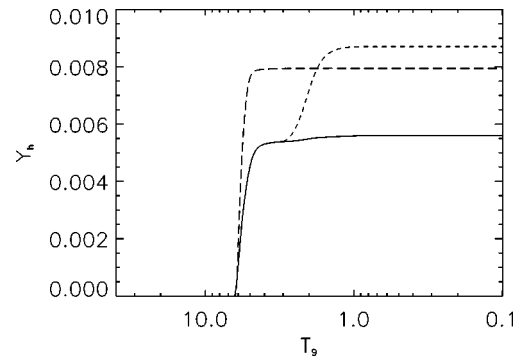


FIG. 7. The abundance of heavy nuclei (i.e., those nuclei with  $A \geq 12$ ) per nucleon for models 0 (solid curve), 1 (dotted curve), 2 (short-dashed curve), and 3 (long-dashed curve). Neutrino capture on free nucleons enhances production of heavy seed nuclei. This strongly reduces the neutron-to-seed ratio  $R$  and limits the  $r$ -process. Notice the rise in  $Y_h$  in the reference calculation (model 0) for  $T_9 \leq 2$ . This results from the late assembly of alpha particles into heavy nuclei via the  $\alpha + \alpha + n \rightarrow {}^9\text{Be}$  followed by  ${}^9\text{Be}(\alpha, n){}^{12}\text{C}$  reaction sequence.

the possibility of making high-mass nuclei by depleting the supply of free neutrons. It also increases  $Y_h$ , the number of heavy nuclei. This in turn lowers  $R$ . Figure 7 shows  $Y_h$  in models 0 through 3. In the reference calculation (model 0),  $Y_h$  rises to about 0.005 at  $T_9=5$  and then increases slowly from that point on. The small rise for  $T_9 \approx 3$  comes from late assembly of heavies via the  $\alpha + \alpha + n$  reaction. Because  $Y_h$  changes only slowly for  $T_9 < 5$ , the nuclear populations are in a large QSE. The subsequent evolution is to break that large QSE into smaller QSE clusters and eventually  $(n, \gamma) - (\gamma, n)$  equilibrium, as described in Sec. IV.

Model 1 behaves exactly the same as model 0, and there is no perceptible difference in the number of heavy nuclei in the two models. In model 2, however, the effect of neutrino capture on free neutrons dramatically increases the number of heavy nuclei for  $T_9 < 3$ . The exact mechanism for production of new heavy nuclei is discussed below in Sec. VI. In model 3, the number of heavy nuclei shoots up between  $T_9 = 6$  and  $T_9 = 5$  to a large value and then stays constant.

The reason for the sudden rise in  $Y_h$  for model 3 may be seen in Fig. 8, which presents the mass fraction of alpha particles for models 0 through 3. First we discuss the other models. The evolution of the alpha particle mass fraction,  $X_\alpha$ , in models 0, 1, and 2 is nearly the same. As  $T_9$  drops below 10, neutrons and protons begin to assemble into alpha particles.  $X_\alpha$  peaks at 0.46 at about  $T_9=7$ . The remaining mass is in free neutrons. This correctly gives  $Y_e = X_\alpha/2 = 0.23$  (cf. Fig. 6).  $X_\alpha$  then falls as the alphas assemble into heavy nuclei. This assembly of heavy nuclei slows down considerably below  $T_9=4$ , and the alphas freeze out with a final mass fraction of about 0.07. In model 2, the neutrino captures on free neutrons causes the alpha mass fraction at first to rise and then to fall. This is related to the production of new heavy nuclei seen in Fig. 7. In model 3, however,  $X_\alpha$  rises to a much higher value and also freezes out at a much higher level. The reason for this is the so-called “alpha effect” [13].

The alpha effect occurs when neutrons and protons assemble into  ${}^4\text{He}$  in the presence of a large flux of neutrinos.

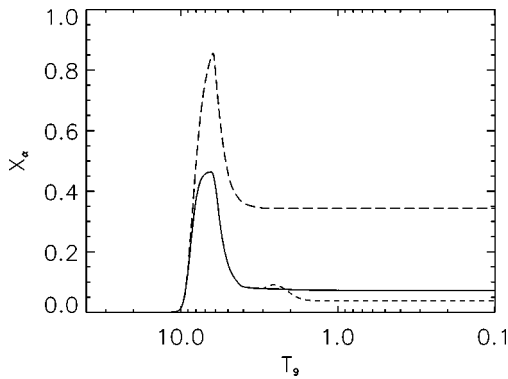


FIG. 8. The mass fraction of alpha particles in models 0 (solid curve), 1 (dotted curve), 2 (short-dashed curve), and 3 (long-dashed curve). In the reference calculation (model 0), the alpha mass fraction grows to a value of about 0.45 ( $T_9 \approx 7$ ) as neutrons and protons assemble into alpha particles and then falls again as the alphas assemble into heavier nuclei. Models 1 and 2 follow suit, although neutrino capture on free neutrons affects the alpha mass for  $T_9 < 3$  in model 2. For model 3, the alpha mass fraction grows to a value larger than 0.8. This is the “alpha effect.” As protons lock up into  $^4\text{He}$  nuclei, which are essentially inert to neutrino capture, ongoing neutrino capture on free neutrons leads to production of new protons which in turn make new alphas. This strongly enhances the resulting alpha mass, increases  $Y_e$ , and reduces  $R$ , the neutron-to-seed ratio.

The interaction of neutrinos with neutrons and antineutrinos with protons sets up a steady-state ratio of the abundance of free neutrons to protons  $Y_n/Y_p$ . In the present models we have initially  $Y_n/Y_p = 3.3$ . At high temperature, only free nucleons are present, so  $Y_n/Y_p = 3.3$  corresponds to  $Y_e = 0.23$ . However, as protons lock up into  $^4\text{He}$ , which is largely inert to the neutrino interactions,  $Y_n/Y_p$  rises rapidly. Neutrino captures on free neutrons will tend to reset  $Y_n/Y_p$  back to 3.3, in accordance with the neutrino temperatures. The newly created protons, however, do not remain free but rather gather into new alpha particles, again upsetting the  $Y_n/Y_p$  ratio. This then establishes a runaway that causes the dramatic rise in  $X_\alpha$  and  $Y_e$ .  $Y_e$  would rise to 0.5 were it not for the fact that heavy nuclei form and soak up free neutrons, thereby limiting the alpha effect runaway. In any event, the alpha effect causes a rapid depletion of free neutrons that kills the possibility of an  $r$ -process.

The average charge  $\langle Z \rangle$  and mass number  $\langle A \rangle$  of heavy nuclei in each of the four models are shown in Fig. 9. The initial build up of heavy nuclei between  $T_9 = 7$  and  $T_9 = 5$  is apparent, as is the subsequent  $r$ -process for models 0 and 1. There is no discernible difference between the final average charge and mass in these two models although neutrino captures do cause the nuclei to work their way up the network faster in model 1. Model 2 has an interesting dip in  $\langle Z \rangle$  and  $\langle A \rangle$  for  $T_9$  between 3 and about 0.5. This results from the assembly of new heavy nuclei already seen in Fig. 7. This creates new and much lighter nuclei than were present for  $T_9 > 3$ , thereby lowering the average charge and mass. Only as the assembly of new seed nuclei shuts off below  $T_9 = 2$  can these quantities again rise by  $r$ -processing. The damage has already been done, however, and the final average charge and mass in model 2 are much less than in models 0 and 1.  $\langle Z \rangle$  and  $\langle A \rangle$  freeze out in model 3 at about  $T_9 = 5$ . In this

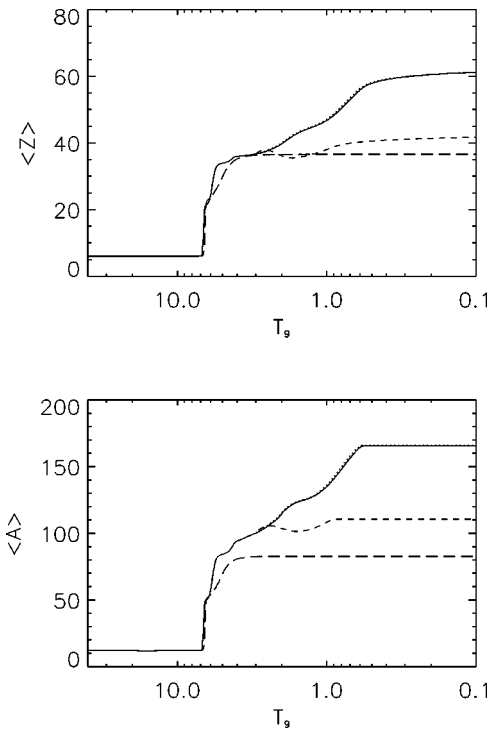


FIG. 9. The average charge  $\langle Z \rangle$  (upper panel) and average mass number  $\langle A \rangle$  (lower panel) of heavy nuclei in models 0 (solid curve), 1 (dotted curve), 2 (short-dashed curve), and 3 (long-dashed curve). In models 0, 1, and 2, the seed nuclei build up to about charge 40 and mass 100 by the onset of the  $r$ -process at  $T_9 \approx 3$ . In models 0 and 1, nuclear beta decays and neutron captures during the  $r$ -process then increase  $\langle Z \rangle$  and  $\langle A \rangle$ . In model 2, however, neutrino capture on free nucleons creates new and lighter seed nuclei. This causes the average charge and mass to drop before climbing again as the assembly of new nuclei ceases. In model 3, the average charge and mass freeze out early because the alpha effect has depleted the supply of light particles.

case, the alpha effect depletes the abundance of light particles and there is little subsequent evolution in the abundances.

In summary, neutrino capture during nucleosynthesis severely hinders the  $r$ -process in the present models. When all neutrino capture effects during nucleosynthesis are included (model 3), no  $r$ -process occurs at all, even though the same calculation without neutrino capture (model 0) at all yields an extremely robust  $r$ -process. The tiny helpful effects of capture on heavy nuclei (model 1) are more than offset by the detrimental effects of capture on free neutrons. This is true even if neutrino capture on free neutrons only occurs during the  $r$ -process phase (model 2).

## VI. ASSEMBLY OF HEAVY NUCLEI

The results in the previous section showed that neutrino-capture enhanced assembly of heavy nuclei strongly hindered the  $r$ -process. In this section we study this in more detail. The goal is to understand exactly how the neutrino capture actually hinders the  $r$ -process.

In the alpha effect, neutrino capture drastically reduces the abundance of free neutrons. It also increases the abundance of alpha particles, which in turn allows assembly of

more seed nuclei. Which of the two effects, loss of neutrons or assembly of new seed nuclei, is the dominant one in limiting the  $r$ -process?

We can understand this as follows. The rate of change of the neutron-to-seed ratio  $R$  is

$$\frac{dR}{dt} = \frac{d(Y_n/Y_h)}{dt} = \frac{1}{Y_h} \frac{dY_n}{dt} - \frac{Y_n}{Y_h^2} \frac{dY_h}{dt}. \quad (26)$$

In order to compute  $dY_n/dt$  and  $dY_h/dt$ , we must consider the fate of a proton newly formed by a neutrino capture on a free neutron. Such a proton will most likely capture two neutrons to become a tritium nucleus. The tritium may then capture another neutrino-capture produced proton in a  $t+p \rightarrow n+{}^3\text{He}$  reaction. The  ${}^3\text{He}$  will then quickly capture another neutron to become  ${}^4\text{He}$ . Alternatively, the tritium may capture another tritium in the reaction  $t+t \rightarrow 2n+{}^4\text{He}$ . In either case, each neutrino capture on a free neutron leads to the disappearance of two free neutrons—the neutron suffering the neutrino capture and the neutron that accompanies it into  ${}^4\text{He}$ . For this reason,

$$\frac{dY_n}{dt} = -2\lambda Y_n, \quad (27)$$

where  $\lambda$  is the rate of neutrino capture on free neutrons. In principle we should include creation of neutrons by antineutrino capture on protons. However the mass fraction of protons becomes negligible as soon as alpha particles form, so we neglect this process in Eq. (27). Furthermore, we neglect in Eq. (27) the loss of free neutrons due to incorporation into nuclei during the  $r$ -process. This loss occurs slowly if the neutrino capture is large.

${}^4\text{He}$  nuclei assembled in this way will tend to react via a three-body reactions to form new heavy nuclei. At late time,  $T_9 < 6$ , some alpha particles will be in existence while some will be created after neutrino captures on neutrons. If  $n$  (where on average  $n \leq 6$ ) neutrino captures are required to produce a new heavy nucleus then,

$$\frac{dY_h}{dt} = \frac{\lambda Y_n}{n}. \quad (28)$$

Substitution of Eqs. (27) and (28) into Eq. (26) then yields

$$\frac{dR}{dt} = -2\lambda R - \frac{\lambda R^2}{n}. \quad (29)$$

The  $R^2$  term in Eq. (29) arises from the assembly of new seed nuclei. It provides the dominant reduction in  $R$  throughout most of the expansion. For example, early in the expansion, when  $R=300$ , say, the assembly of new seed nuclei induced by neutrino capture causes  $R$  to decline at a rate about 15 000 times faster than the rate of neutrino capture on free neutrons. This explains the extremely fast drop in  $R$  in model 3 seen in Fig. 5. Only as  $R$  drops below 10 does the simple disappearance of neutrons cause a larger drop in  $R$ . These considerations explain why the alpha effect is so devastating to the  $r$ -process.

Model 2 also shows a rapid drop in  $R$  and a rapid increase in the number of heavy nuclei after neutrino capture on free

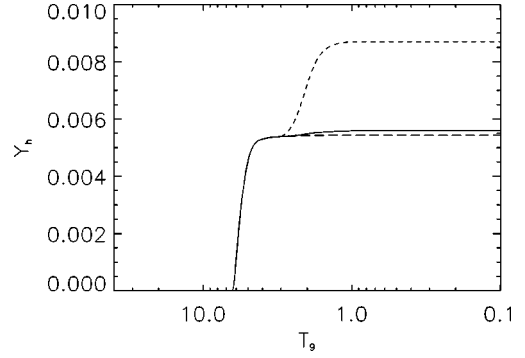


FIG. 10. The abundance of heavy nuclei  $Y_h$  in models 0 (solid line), 2 (short-dashed curve), and 4 (long-dashed curve). Model 4 is identical to model 2 except that the reaction  ${}^3\text{H}(\alpha, \gamma){}^7\text{Li}$  has been disabled. This prevents assembly of new seed nuclei induced by neutrino capture on free neutrons. When the  ${}^7\text{Li}$  channel is open (model 2),  $Y_h$  grows dramatically.

neutrons turns on at  $T_9=3$ . This is perhaps surprising since the three-body reactions assembling heavy nuclei from alpha particles are rather slow at this temperature. It indicates that another channel has opened for the assembly of seed nuclei.

Another possible fate of a tritium nucleus formed via neutrino capture on a free neutron is to capture one of the abundant alpha particles to become  ${}^7\text{Li}$  which can then capture other light particles to assemble new heavy nuclei. This does not happen immediately in model 2, however. At  $T_9 \approx 3$ , the  $(\gamma, \alpha)$  reaction on  ${}^7\text{Li}$  is rapid and keeps the net  ${}^3\text{H}(\alpha, \gamma){}^7\text{Li}$  rate low. This allows tritium to move into  ${}^4\text{He}$ . As the temperature drops, the disintegration of  ${}^7\text{Li}$  slows, and tritium increasingly captures to  ${}^7\text{Li}$ . This leads to significant assembly of new heavy nuclei (Fig. 7), which again poisons the  $r$ -process by decreasing  $R$ .

That this is indeed the mechanism for assembly of new heavy nuclei is apparent from Fig. 10. This figure shows  $Y_h$  during models 0 (solid curve), 2 (short-dashed curve), and 4 (long-dashed curve). Model 4 was identical to model 2 (neutrino capture on free nucleons and heavy nuclei below  $T_9=3$ ) except that the  $t+{}^4\text{He} \rightarrow {}^7\text{Li}$  reaction was disabled. Few new seed nuclei assemble in model 4 because the three-body reactions are slow and the  ${}^7\text{Li}$  channel is closed. In this case, neutrino capture on free neutrons simply leads to a substantial increase in the mass fraction of alpha particles, as is apparent in Fig. 11. Because the free neutrons rapidly disappear in model 4 below  $T_9=3$ , the  $\alpha + \alpha + n$  reaction is very slow, and model 4 ends up with even fewer heavy nuclei than model 0. In spite of this, the neutrino capture means the  $r$ -process is less robust in model 4 than in model 0.

As a final point, the late assembly of new seed nuclei through the  ${}^7\text{Li}$  channel will happen even if no  ${}^4\text{He}$  nuclei initially are present. Once neutrino capture on free neutrons turns on, the  ${}^4\text{He}$  abundance will grow until it is sufficiently large to allow the  ${}^3\text{H}(\alpha, \gamma){}^7\text{Li}$  reaction to proceed rapidly. Thus, late assembly of seed nuclei will occur even in low-entropy  $r$ -processes (for which the alpha abundance is initially very low) if the neutrino flux is large.

## VII. NEUTRINO CAPTURE AND QSE

The alpha effect and ongoing neutrino capture on free neutrons essentially precludes the possibility of accelerating

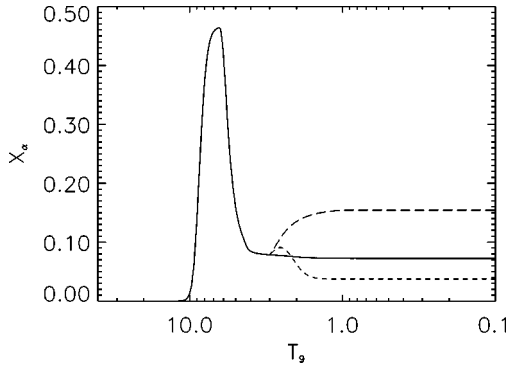


FIG. 11. The mass fraction of  ${}^4\text{He}$  in models 0 (solid line), 2 (short-dashed curve), and 4 (long-dashed curve). Model 4 is identical to model 2 except that the reaction  ${}^3\text{H}(\alpha, \gamma){}^7\text{Li}$  has been disabled. This prevents assembly of new seed nuclei induced by neutrino capture on free neutrons. The fate of a proton produced from neutrino capture on a free neutron is thus to end up as a  ${}^4\text{He}$  nucleus, hence the rise in  $X_\alpha$  in model 4.

the  $r$ -process via strong neutrino capture on heavy nuclei. Nevertheless, it is interesting to consider what the effect of neutrino capture on heavy nuclei alone would do in an intense neutrino flux.

One might suppose that allowing neutrino capture on heavy nuclei to occur earlier in the expansion than  $T_9=3$  as in model 1 would help the  $r$ -process. Earlier neutrino capture would move nuclei to higher mass earlier and possibly accelerate the  $r$ -process. In fact the opposite is true and points out the importance of the QSE concept in considerations of neutrino capture during the  $r$ -process.

To test the effect of neutrino capture on heavy nuclei, we ran models 5, 6, and 7, which were identical to model 1 except that they used a larger neutrino luminosity of  $L_\nu = 10^{52}$  ergs/s for electron neutrinos and  $L_{\bar{\nu}_e} = 4 \times 10^{52}$  ergs/s for the electron antineutrinos and that, respectively, they allowed neutrino capture only on heavy nuclei to begin at  $T_9=7$ ,  $T_9=5$ , and  $T_9=3$ . The larger luminosity increases the neutrino capture and thereby shows the effects more clearly. (Indeed, without the increased neutrino luminosities, we saw little effect even if the neutrino capture on nuclei was on throughout the expansion.) Since no heavy nuclei exist prior to  $T_9=7$ , model 5 is equivalent to having neutrino capture on heavy nuclei on throughout the expansion.

Figure 12 compares  $Y_e$  in models 5, 6, and 7 to that in model 0. As is evident, allowing neutrino capture to occur earlier does cause  $Y_e$  to rise much earlier in the expansion. It also causes  $R$  to drop much more rapidly, as seen in Fig. 13. This does not, however, correspond to a more robust  $r$ -process in models 5 and 6. Figure 14 shows  $\langle Z \rangle$  and  $\langle A \rangle$  for models 0, 5, 6, and 7, and it is readily apparent that early neutrino capture on heavy nuclei alone in fact tends to hinder the  $r$ -process. This result may seem counterintuitive, so we study it in a little more detail.

As discussed in Sec. IV, the nuclei begin in NSE at high temperature. As the temperature falls, the NSE breaks down (at  $T_9 \approx 6-7$  in the present calculations). The system descends the hierarchy of statistical equilibria and goes into a QSE in which the heavy nuclei are all in equilibrium under exchange of light particles. In the present calculations, a

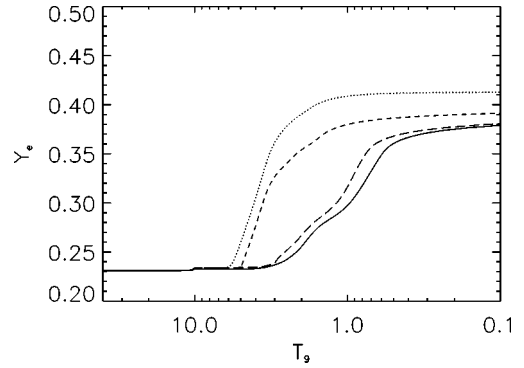


FIG. 12.  $Y_e$  during the expansion for models 0 (solid curve), 5 (dotted curve), 6 (short-dashed curve), and 7 (long-dashed curve). In models 5, 6, and 7, there is only neutrino capture on heavy nuclei for  $T_9 < 7$ ,  $T_9 < 5$ , and  $T_9 < 3$ , respectively. The earlier the neutrino capture is allowed to occur, the earlier  $Y_e$  rises. This does not translate into an increase in the average charge and mass of the heavy nuclei, however (see Fig. 14).

large QSE containing the most abundant nuclei persists down to  $T_9 \approx 4.0$  after which point an increasing number of smaller QSE clusters appears. Eventually these evolve to the  $(n, \gamma) - (\gamma, n)$  equilibria that represent the classical  $r$ -process phase of the expansion. The crucial point for neutrino capture is that even below  $T_9 \approx 5$ , the nuclear abundances are interlocked. This means that any increase in  $Y_e$  via a neutrino capture can cause a readjustment of all nuclear abundances, not just that of the neutrino-capturing nucleus.

The QSE-nature of the abundance distributions for  $T_9 \approx 5$  explains the larger final mass fraction of alpha particles in models with earlier capture on heavy nuclei, as seen in Fig. 15. As the nuclei capture neutrinos, they become more proton rich. In doing so, the average binding of protons in nuclei decreases. In the QSE, then, the abundance of free protons tends to increase. In practice, the lower proton binding means the average rate of proton disintegration reactions

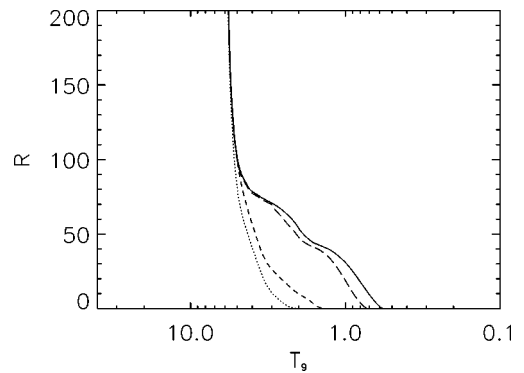


FIG. 13.  $R$  during the expansion for models 0 (solid curve), 5 (dotted curve), 6 (short-dashed curve), and 7 (long-dashed curve). In models 5, 6, and 7, there is only neutrino capture on heavy nuclei for  $T_9 < 7$ ,  $T_9 < 5$ , and  $T_9 < 3$ , respectively.  $R$  declines sharply due to neutrino capture on heavy nuclei alone. This does not lead to a more robust  $r$ -process, however. When the neutrino capture occurs during the QSE phase of the expansion, the equilibrium among heavy nuclei allows neutrons to convert rapidly into protons without increasing the average charge. This decreases  $R$  and hinders the  $r$ -process.

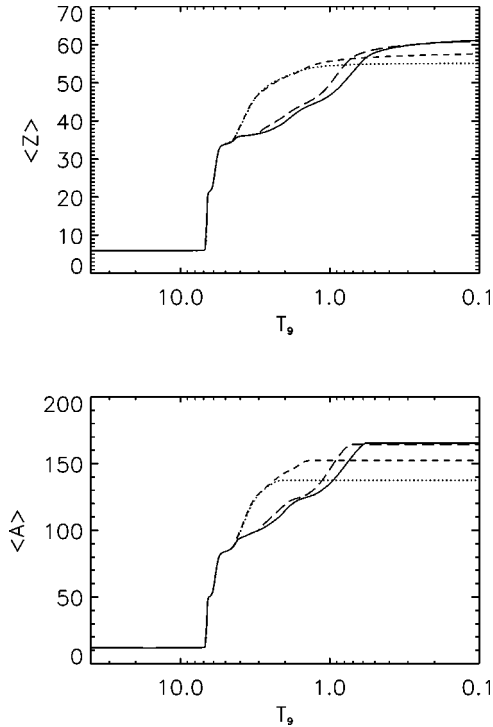


FIG. 14. Average charge  $\langle Z \rangle$  (top panel) and average mass number  $\langle A \rangle$  (bottom panel) of heavy nuclei during the expansion for models 0 (solid curve), 5 (dotted curve), 6 (short-dashed curve), and 7 (long-dashed curve). Stronger neutrino capture by heavy nuclei limits the  $r$ -process if the captures happen during the QSE phases of the expansion.

on heavy nuclei increases somewhat. The protons, however, are also in equilibrium with neutrons and alpha particles; therefore, an increase in the free proton abundance causes the alpha mass also to increase. The increased alpha mass then leads to further assembly of heavy nuclei via the three-body reaction channels. This is apparent in Fig. 16.

Figure 17 shows the final abundances versus nuclear mass for models 0, 5, 6, and 7. The hindrance of the  $r$ -process in models 5 and 6 is readily apparent. Model 7, however, is little different from model 0, even though the  $r$ -process was

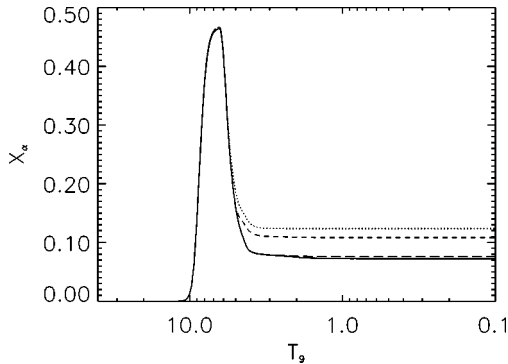


FIG. 15. The mass fraction of alpha particles during the expansion for models 0 (solid curve), 5 (dotted curve), 6 (short-dashed curve), and 7 (long-dashed curve). In models 5, 6, and 7, there is only neutrino capture on heavy nuclei for  $T_9 < 7$ ,  $T_9 < 5$ , and  $T_9 < 3$ , respectively. Neutrino captures on heavy nuclei increases  $Y_e$ . This tends to increase the abundance of free protons in the QSE. The protons capture neutrons and increase the abundance of  ${}^4\text{He}$ .

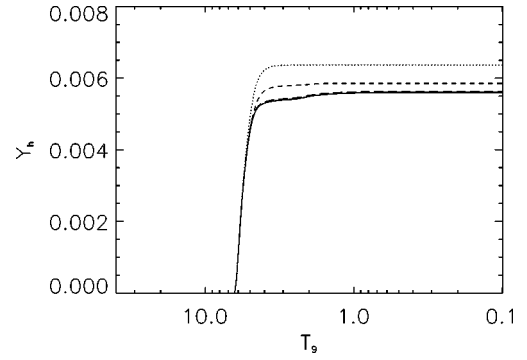


FIG. 16.  $Y_h$  during the expansion for models 0 (solid curve), 5 (dotted curve), 6 (short-dashed curve), and 7 (long-dashed curve). In models 5, 6, and 7, there is only neutrino capture on heavy nuclei for  $T_9 < 7$ ,  $T_9 < 5$ , and  $T_9 < 3$ , respectively. The increased production of alpha particles due to neutrino capture on heavy nuclei (see Fig. 15) increases the production of heavy nuclei via the three-body reaction sequences  $\alpha + \alpha + \alpha \rightarrow {}^{12}\text{C}$  and  $\alpha + \alpha + n \rightarrow {}^9\text{Be}$  followed by  ${}^9\text{Be} + \alpha \rightarrow {}^{12}\text{C} + n$ .

accelerated by neutrino captures on nuclei. As stated previously, it is the neutron-to-seed ratio  $R$  that determines the robustness of an  $r$ -process. Because the neutrino capture on nuclei in model 7 happens after the large QSE has broken down into  $(n, \gamma) - (\gamma, n)$  equilibrium clusters, there is little effect on  $R$ . The result is that nuclei capture almost exactly the same average number of neutrons per nucleus in models 0 and 7. That the final abundance distributions for these models are so similar shows that at this flux, neutrino capture is not very significant compared to nuclear beta decay during the  $r$ -process phase.

## VIII. IMPLICATIONS

The essential conclusion of our work is that, given standard neutrino physics and a realistic neutrino-driven wind, strong neutrino capture hinders the  $r$ -process. This can happen in several ways. The largest effects come from neutrino capture on free neutrons during the stages of alpha particle and heavy nucleus formation. Furthermore, a strong neutrino flux will also impede the  $r$ -process by inducing significant neutrino capture on heavy nuclei while the material is still in QSE ( $T_9 > 4$ ). Although neutrino capture on heavy nuclei after  $T_9 < 3$  is not necessarily problematic, the simultaneous capture on free neutrons is detrimental. In order to examine the effects of charged-current neutrino interactions on  $r$ -process synthesis, it is necessary to take into account feedback between nuclear dynamics and weak interactions. Also, because neutrino-capture effects at a late stage in the expansion imply larger effects at earlier stages in the expansion (absent neutrino flavor/type transformation effects), neutrino interactions must be self-consistently included everywhere.

The effects we have described pose a severe challenge to the  $r$ -process in stellar explosions. The  $r$ -process components that produced the solar system's supply of platinum and gold must have taken place in a sufficiently low flux of normal electron neutrinos that a strong alpha effect did not occur. We conclude that either (1) the  $r$ -process occurred in an environment not associated with a strong  $\nu_e$  flux, or (2) in supernovae fluid elements are carried away extremely rap-

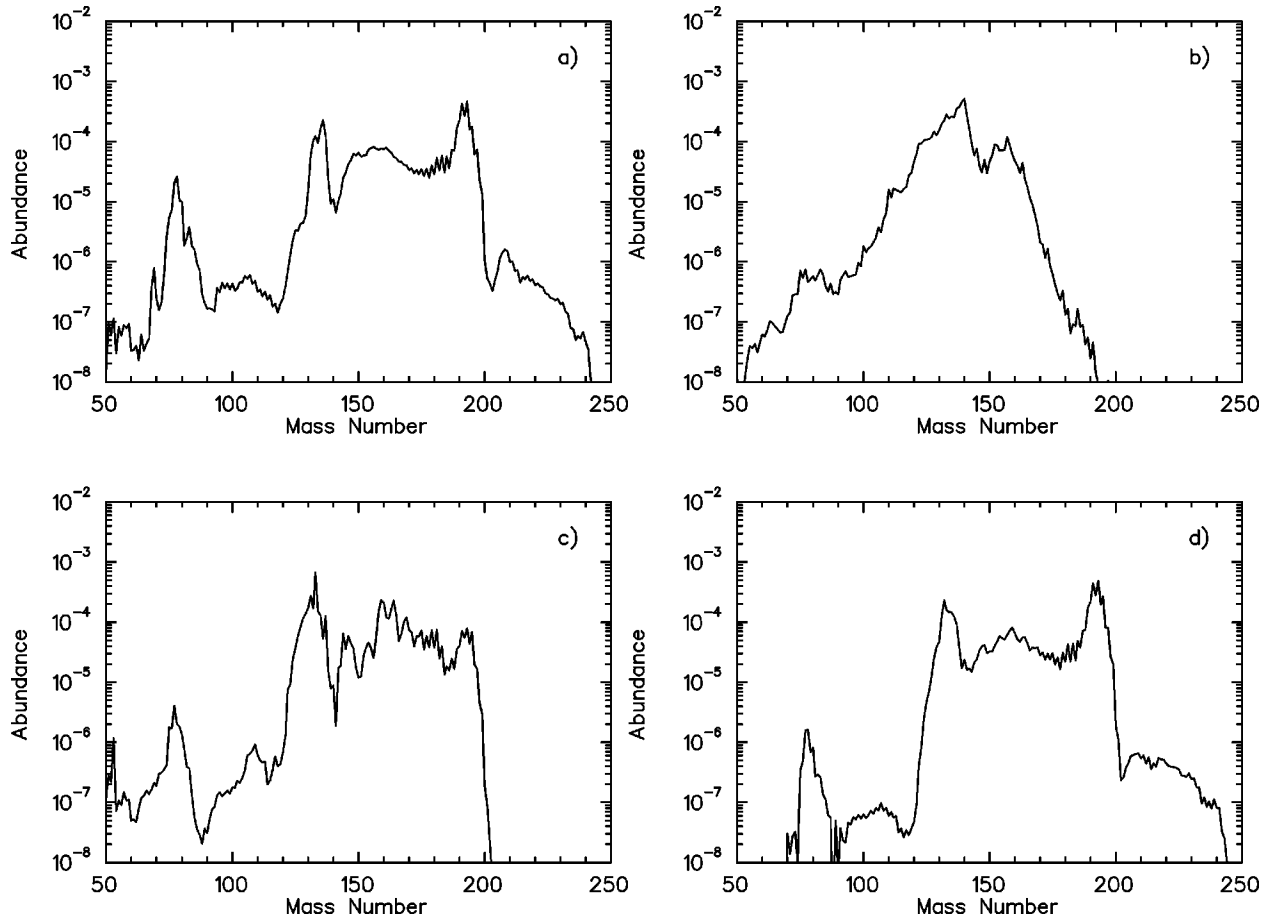


FIG. 17. The final mass fractions vs nuclear mass number for (a) model 0, (b) model 5, (c) model 6, and (d) model 7. Neutrino capture on heavy nuclei during the QSE phase of the expansion has hindered the  $r$ -process in models 5 and 6.

idly to regions where the  $\nu_e$  flux is low, or (3) some non-standard neutrino effects are present. While we have employed an exponential outflow model with particular entropy and neutrino fluxes in this paper, our qualitative conclusions regarding the effects of charged-current neutrino processes will hold for any general outflow model.

In fact, however, any attempt to circumvent the harmful influence of the alpha effect by invoking convection (or multidimensional hydrodynamics) or general relativity will be problematic. This stems from the fact that it is the weak interaction (changing neutrons to protons and vice versa) that is at the heart of the troubles with the  $r$ -process conditions. Any model that uses neutrino interactions to supply the requisite energy to eject nucleons from deep in the gravitational potential well of the neutron star will necessarily also have the  $Y_e$  of the ejecta set by the neutrino capture competition between the processes in Eqs. (1) and (2). This is because a nucleon near the surface of the neutron star has a typical binding energy of  $\sim 100$  MeV, implying that it must suffer  $\sim 5$  neutrino interactions to be ejected to interstellar space. Necessarily, this also implies that the alpha effect and other deleterious effects of  $\nu_e$  interactions on nucleosynthesis can operate. If one wants the material to be ejected on such a short time scale that  $\nu_e$  capture cannot ruin  $r$ -process nucleosynthesis, then one would be forced to find an energy source for the ejection process that would not be based on neutrino heating. In turn, this may be difficult to engineer because almost all of the energy available to the supernova resides in

the neutrino seas. In this case one would have to utilize, for example, rotational energy in the core, as in a Leblanc-Wilson jet [24]. This would mean giving up on the neutrino-driven wind model predictions of  $r$ -process yields per supernova which naturally agree with observationally-inferred galactic heavy element chemical evolution constraints (e.g., [3,4]).

Neutrino-driven wind models including general relativistic effects have been investigated as a method for increasing the neutron-to-seed ratio and facilitating the  $r$ -process [9,10]. These models have the effect of decreasing the time scale and increasing the entropy. An alpha effect will also occur in these models. The degree to which it impacts the nucleosynthesis products needs to be investigated. However, such general relativistic extensions of neutrino driven wind models suffer from additional problems such as a requirement for fine tuning of mass ejection rates and differential neutrino gravitational redshift.

An alternative idea is that nonstandard neutrino physics may allow  $r$ -processing even in a high neutrino flux. For example, if most electron neutrinos were converted to other neutrino species (either active or sterile) by matter-enhanced processes in the region above the neutron star surface [25,26], the initial neutron richness would be quite large because a large flux of antineutrinos would drive protons into neutrons. Additionally, a reduced  $\nu_e$  flux would preclude reducing this large neutron excess by driving the neutrons back into protons. Furthermore, no alpha effect would occur when

nucleosynthesis begins. Many scenarios of this type exist and merit investigation, although we again caution one must include all neutrino effects and must properly take the nuclear dynamics into account.

The strong sensitivity of  $r$ -process yields to the neutrino flux present interesting implications for the extinct  $r$ -process radioactivities. Chief among these isotopes are  $^{129}\text{I}$  and  $^{182}\text{Hf}$ , with half-lives of 16 Myr and 9 Myr, respectively. Meteoritical evidence indicates that these isotopes were alive in the early solar system, an observation that apparently constrains galactic nucleosynthesis over the last several million years prior to collapse of the solar nebula. The curious aspect of these isotopes is that the inferred live  $^{182}\text{Hf}$  abundance in the early solar system roughly agrees with expectations from continuous galactic nucleosynthesis while the inferred  $^{129}\text{I}$  abundance fails to reach the same expectations by about a factor of 100. An obvious explanation is that there are different kinds of supernovae which occur with different frequencies [27,28].

In any case, perhaps the clues about the  $r$ -process synthe-

sis rates in the galaxy provided by considering  $^{129}\text{I}$  and  $^{182}\text{Hf}$  could give us insights into how nature manages to circumvent the alpha effect. It could be that the supernova events that are responsible for the production of  $^{129}\text{I}$  represent only a "partial"  $r$ -process where vigorous neutron capture to or beyond mass 130 is hindered by the alpha effect. Likewise the  $^{182}\text{Hf}$  production events have somehow managed to completely disable the alpha effect.

In summary, strong neutrino capture during expansions of neutron-rich matter greatly hinders production of  $r$ -process isotopes. It will be fascinating to see how this dramatic conclusion will lead to new insights into supernova dynamics, neutrino physics, and the  $r$ -process of nucleosynthesis.

#### ACKNOWLEDGMENTS

This work was supported in part by NASA Grant No. NAGW-3480 at Clemson and NSF Grant PHY95-03384 at UC San Diego.

- 
- [1] E. M. Burbidge, G. R. Burbidge, W. A. Fowler, and F. Hoyle, *Rev. Mod. Phys.* **29**, 547 (1957).
- [2] For a review of the  $r$ -process, see J. J. Cowan, F.-K. Thielemann, and J. W. Truran, *Phys. Rep.* **208**, 267 (1991); B. S. Meyer, *Annu. Rev. Astron. Astrophys.* **32**, 153 (1994); or G. Wallerstein *et al.*, *Rev. Mod. Phys.* **69**, 995 (1997).
- [3] S. E. Woosley and R. D. Hoffman, *Astrophys. J.* **395**, 202 (1992).
- [4] B. S. Meyer, G. J. Mathews, W. M. Howard, S. E. Woosley, and R. D. Hoffman, *Astrophys. J.* **399**, 656 (1992).
- [5] W. M. Howard, S. Goriely, M. Rayet, and M. Arnould, *Astrophys. J.* **417**, 713 (1993).
- [6] K. Takahashi, J. Witt, and H.-T. Janka, *Astron. Astrophys.* **286**, 857 (1994).
- [7] S. E. Woosley, G. J. Mathews, J. R. Wilson, R. D. Hoffman, and B. S. Meyer, *Astrophys. J.* **433**, 229 (1994).
- [8] Y.-Z. Qian, G. M. Fuller, G. J. Mathews, R. W. Mayle, J. R. Wilson, and S. E. Woosley, *Phys. Rev. Lett.* **71**, 1965 (1993).
- [9] C. Y. Cardall, G. M. Fuller, *Astrophys. J. Lett.* **486**, L111 (1997).
- [10] Y.-Z. Qian and S. E. Woosley, *Astrophys. J.* **471**, 331 (1996).
- [11] Y.-Z. Qian, W. C. Haxton, K. Langanke, and P. Vogel, *Phys. Rev. C* **55**, 1532 (1997).
- [12] B. S. Meyer, *Astrophys. J. Lett.* **449**, 55 (1995).
- [13] G. M. Fuller and B. S. Meyer, *Astrophys. J.* **453**, 792 (1995).
- [14] G. McLaughlin, G. M. Fuller, and J. R. Wilson, *Astrophys. J.* **472**, 440 (1996).
- [15] G. McLaughlin and G. M. Fuller, *Astrophys. J.* **489**, 766 (1997).
- [16] D. K. Nadyozhin and I. V. Panov, in *Proceedings of the International Symposium on Weak and Electromagnetic Interactions in Nuclei* (WEIN-92), edited by Ts. D. Vylov (World Scientific, Singapore, 1993), p. 479.
- [17] B. S. Meyer, in *Intersections Between Particle and Nuclear Physics*, edited by T. W. Donnelly (AIP, Woodbury, 1997), p. 992.
- [18] G. McLaughlin and G. M. Fuller, *Astrophys. J.* **455**, 202 (1995).
- [19] R. C. Duncan, S. L. Shapiro, and I. Wasserman, *Astrophys. J.* **309**, 141 (1986).
- [20] B. S. Meyer, T. D. Krishnan, and D. D. Clayton, *Astrophys. J.* **462**, 825 (1996).
- [21] B. S. Meyer, T. D. Krishnan, and D. D. Clayton, *Astrophys. J.* **498**, 808 (1998).
- [22] B. S. Meyer and J. S. Brown, *Astrophys. J., Suppl. Ser.* **112**, 199 (1997).
- [23] D. Bodansky, D. D. Clayton, and W. A. Fowler, *Astrophys. J., Suppl.* **16**, 299 (1968).
- [24] J. M. LeBlanc and J. R. Wilson, *Astrophys. J.* **161**, 541 (1970).
- [25] D. O. Caldwell, G. M. Fuller, and Y.-Z. Qian, *Phys. Rev. D* (submitted).
- [26] G. C. McLaughlin, J. Fetter, B. Balantekin, and G. M. Fuller, *Phys. Rev. D* (submitted).
- [27] G. J. Wasserburg, M. Busso, and R. Gallino, *Astrophys. J. Lett.* **466**, L109 (1996).
- [28] Y.-Z. Qian, P. Vogel, and G. J. Wasserburg, *Astrophys. J.* **494**, 285 (1998).